Landau levels from neutral Bogoliubov particles in two-dimensional nodal superconductors under strain and doping gradients

Emilian M. Nica[*] and Marcel Franz

Department of Physics and Astronomy and Quantum Matter Institute, University of British Columbia,
Vancouver, British Columbia, Canada V6T 1Z1

Motivated by recent work on strain-induced pseudomagnetic fields in Dirac and Weyl semimetals, we analyze the possibility of analogous fields in two-dimensional nodal superconductors. We consider the prototypical case of a d-wave superconductor, a representative of the cuprate family, and find that the presence of weak, spatially varying strain leads to pseudomagnetic fields and Landau quantization of Bogoliubov quasiparticles in the low-energy sector. A similar effect is induced by the presence of generic, weak doping gradients. In contrast to genuine magnetic fields in superconductors, the strain- and doping-gradient-induced pseudomagnetic fields couple in a way that preserves time-reversal symmetry and is not subject to the screening associated with the Meissner effect. These effects can be probed by tuning weak applied supercurrents which lead to shifts in the energies of the Landau levels and hence to quantum oscillations in thermodynamic and transport quantities.

I. INTRODUCTION

Elementary excitations in superconductors are composed of coherent superpositions of electron and hole degrees of freedom [1–3]. These Bogoliubov quasiparticles are electrically neutral on average and therefore do not couple simply to the externally applied magnetic field. In addition, superconductors are known either to expel magnetic field from their bulk completely [4] or to form a flux lattice [5], in which the quasiparticle dynamics is effectively zero field [6]. For these reasons superconductors normally avoid formation of Landau levels which represent the canonical response of most other electron systems to magnetic field [7].

In this work, we show that weak, spatially varying in-plane strains and doping gradients generically lead to Landau quantization of Bogoliubov quasiparticles for a broad class of two-dimensional (2D) nodal superconductors (SCs). In these cases, the Dirac-like quasiparticles in the vicinity of point nodes are subject to emergent vector potentials which enter in a time-reversal-invariant way. In contrast to genuine magnetic fields in a SC, there are no induced currents and no screening associated with the Meissner effect. Our work is motivated by interesting developments in graphene [8], in which strain-induced pseudomagnetic fields lead to Landau quantization and quantum oscillations, which were already observed in experiment [9], and more recent proposals in the context of Dirac and Weyl semimetals [10–15]. In contrast to Ref. [16], which considered superconducting instabilities of a Landau-quantized normal state in graphene, our proposal involves the emergence of Landau levels directly in the superconducting state and is not dependent on the pairing mechanism.

A possible experimental setup is shown in Fig. 1. Since the most immediate realization of gapless, effectively two-dimensional superconductivity is provided by the broad class of Cu-based materials, we study the case of a prototypical d-wave SC. Strain can be induced, in principle, by allowing for the controlled deformation of an underlying substrate [17–19]. Controlled doping gradients [20,21] provide an alternate way of introducing unconventional vector potentials. As discussed in greater detail in the following, an additional application of a weak supercurrent provides a simple way to detect the underlying quantum oscillations.

In Sec. II we discuss our prototypical model Hamiltonian and show that effective vector potentials emerge in the low-energy limit under weak applied strain or doping gradients. In Sec. III, we present the results of our numerical calculations, which confirm the presence Landau levels in a lattice model. A summary and outlook are provided in Sec. IV. Technical details are relegated to the Appendixes.

II. VECTOR POTENTIALS FROM LATTICE DEFORMATIONS AND DOPING GRADIENTS

Consider a prototypical Hamiltonian [22] on the square lattice $\hat{H} = \hat{H}_{TB} + \hat{H}_\Delta$ corresponding to a nearest-neighbor (NN) tight-binding (TB) part, together with a pairing potential at mean-field level for next-nearest neighbors (NNN). The latter is chosen to belong to the d_{xy} representation of the D_{4h} point group. In momentum space, the Nambu form of the lattice Hamiltonian is written as $\hat{H} = \sum_k \Psi_k^\dagger \mathcal{H}(k)\Psi_k$, with $\Psi_k = (c_{k,\uparrow}, c_{k,\downarrow}, c_{-k,\uparrow}^\dagger, c_{-k,\downarrow}^\dagger)^T$ being the Nambu spinor and

$$\mathcal{H}(k) = h_k \sigma_0 \tau_z + \Delta_k(i\sigma_y)(i\tau_y). \tag{1}$$

Here $\boldsymbol{\sigma}$ and $\boldsymbol{\tau}$ are Pauli matrices in spin and Nambu space, respectively, $h_k = 2t[\cos(k_x a) + \cos(k_y a)] - \mu$, and $\Delta_k = 4\Delta \sin(k_x a) \sin(k_y a)$. In addition, t and Δ are the unperturbed hopping coefficients and pairing amplitudes, respectively, and a is the pristine NN lattice spacing. This choice of Hamiltonian is convenient for carrying out numerical calculations. Other

---

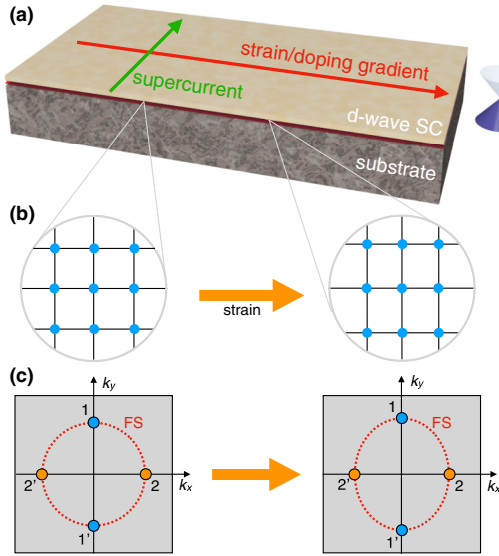*Corresponding author: enica@qmi.ubc.ca

024520-1

FIG. 1. (a) Sketch of a possible experimental setup. The red arrow indicates the direction of variation of either the strain or doping gradient. The green arrow indicates an applied supercurrent. (b) Schematic deformation of the 2D square lattice for the case of uniaxial strain as a function of x alone. (c) The corresponding Fermi surface deforms, and the nodal points, labeled $(1,1')$ and $(2,2')$, move, mimicking the action of a pseudovector potential.

models involving possible $d_{x^2-y^2}$ pairing and different Fermi surfaces lead to similar results, provided nodal quasiparticles are present.

In the absence of any perturbation and below half filling, the low-energy spectrum of $\hat{H}$ is Dirac-like,

$$E_{\boldsymbol{q}}^{(\alpha)} = \pm\sqrt{v_F^2 q_{x/y}^2 + v_\Delta^2 q_{y/x}^2},\qquad(2)$$

about four nodes located at $\boldsymbol{K}_\alpha \in \{(\pm K_F,0),(0,\pm K_F)\}$, where K_F is the Fermi wave vector. We label the pairs of opposite momenta as $\alpha \in \{1,1'\}$ for the nodes along the k_y axis and $\alpha \in \{2,2'\}$ for the nodes along the k_x axis in the Brillouin zone, as shown in Fig. 1(c). We also define the effective Fermi velocities $v_F = 2ta\sin(K_F a), v_\Delta = 4\Delta a\sin(K_F a)$.

We model an arbitrary lattice deformation via the transformation

$$\boldsymbol{R}_i \rightarrow \boldsymbol{R}_i' = \boldsymbol{R}_i + \boldsymbol{u}(\boldsymbol{R}_i),\qquad(3)$$

where $\boldsymbol{R}_i$ are Bravais lattice vectors and $\boldsymbol{u}(\boldsymbol{R}_i)$ are position-dependent displacements of the orbitals. We assume that both NN hopping coefficients and NNN pairing amplitudes are continuous functions of the deformation. While in practice they can be quite sensitive to the details of the material at hand, we assume that the effect of a deformation can be generically modeled by considering the leading contributions in a gradient expansion of a deformation field $\boldsymbol{u}(\boldsymbol{r})$. In addition, we also assume that the leading effect can be captured by a net change in NN bond length, by analogy with the case of graphene [23,24]. We also ignore the contributions from the change in pairing, which are expected to be subleading. While we expect that none of these approximations are crucial for the study of the effect at hand, they provide for a much more transparent discussion.

The pairing potential connects states in the vicinity of pairs of opposite Fermi wave vectors. Consequently, we can focus on the $(1,1')$ pair of nodes.

In the low-energy continuum limit, the Hamiltonian reduces to $H^{(1,1')} = \int d^2r\,\Psi_{\boldsymbol{r}}^\dagger\mathcal{H}\Psi_{\boldsymbol{r}}$, with

$$\mathcal{H} = v_F\left(\sigma_z\tau_0 i\partial_y + \sigma_0\tau_z\frac{e\mathcal{A}_y}{v_F}\right) - v_\Delta\sigma_x\tau_x i\partial_x,\qquad(4)$$

where $\hbar$ has been set to 1 for simplicity. A detailed derivation of this Hamiltonian is provided in Appendix A, but the origin of the vector potential can be understood intuitively by inspecting Figs. 1(b) and 1(c). Note that $\boldsymbol{\sigma}$ are now Pauli matrices in *combined* valley and spin space, and $\Psi_{\boldsymbol{r}} = (\Psi_\uparrow^{(1)},\Psi_\downarrow^{(1')},\Psi_\uparrow^{(1),\dagger},\Psi_\downarrow^{(1'),\dagger})$ is the corresponding Nambu spinor. The Fermi fields are defined for the pristine system in the vicinity of the nodes in standard fashion. Notice that both kinetic and pairing parts are effectively one-dimensional in this limit. Consequently, the deformation-induced potentials, which couple in a gauge-invariant way, are of the form $\mathcal{A} = (0,\mathcal{A}_y)$. The effective one-dimensional form also precludes the emergence of scalar potentials for a generic deformation, in contrast to the case of graphene [8,25,26], where this holds only for pure shear deformations. The effective Hamiltonian about the other two Fermi wave vectors can be obtained by transforming $x \leftrightarrow y$.

Under our assumptions, the generic form of the vector potentials is (see Appendix A)

$$\mathcal{A}_y = \left(\frac{2t\beta}{e}\right)[u_{xx} + \cos(K_F a)u_{yy}],\qquad(5)$$

where $u_{ij} = (1/2)(\partial_j u_i + \partial_i u_j)$ is a symmetric strain tensor and $\beta = d\ln t/d\ln a$ is a standard parameter [24]. Quite generally, the elements of the strain tensor can be continuous functions of (x,y). We list three limiting cases which are more conveniently achieved in numerical calculations and possible experimental setups: (i) *uniaxial strain*, $u_{xx} \neq 0, u_{yy} = 0$; (ii) *hydrostatic compression/dilation*, $u_{xx} = u_{yy}$; and (iii) *pure shear strain*, $u_{xx} = -u_{yy}$. In the following, we shall focus on case (iii), although this does not essentially modify the results.

A very similar form is obtained for the case of a doping gradient in the low-energy limit. This possibility can be modeled by introducing a slow variation of the chemical potential on the scale of the intersite separation. In the low-energy, continuum limit we approximate $\mu \rightarrow \mu[1 + g(\boldsymbol{r})]$. As for the case of lattice deformations, the additional term leads to the emergence of vector potentials of the form

$$\mathcal{A}_y = \left(\frac{\mu}{e}\right)g(\boldsymbol{r}).\qquad(6)$$

This again can be understood intuitively by noting that the doping gradient changes the Fermi surface volume and thus moves the nodal points in the momentum space.

The vector potentials in Eqs. (5) and (6) can lead to pseudomagnetic fields, provided that $\mathcal{B} = \nabla \times \mathcal{A} \neq 0$. For clarity, we analyze the case of strains with monotonic linear variation with distance along x and perform an analogous analysis for the chemical potential case. This corresponds to uniform pseudomagnetic fields. The presence of weak modulations in the strain- or doping-gradient-induced fields does not qualitatively change our conclusions. To ensure that

the continuum limit is a good approximation of the perturbed finite-size system, we require that the components of the vector potentials remain small over the entire sample.

The vector potential terms are invariant under the time-reversal operation, which effectively interchanges the valley and spin indices of the paired fields. Consequently, the Hamiltonian in Eq. (4) is also invariant under time reversal. This ensures that the current density associated with either the deformation or doping gradient vanishes. An important consequence of this is the absence of screening currents and hence of the Meissner effect, which would otherwise prevent the emergence of Landau levels (LLs). We also note that, from a generic Landau-Ginzburg perspective, there is no analog for the standard London equations as the effective strain-induced vector potentials are not determined from the standard gauge-invariant action. Instead, they are derived from a linear-elastic theory, as noted in the case of graphene [24]. Similar arguments hold for doping gradient-induced vector potentials.

The solutions to Eq. (4) can be obtained via a canonical Bogoliubov–de Gennes (BdG) transformation [2]. For node 1 the BdG equations are

$$-\left[v_\Delta i \partial_x \sigma_x + v_F \left(i \partial_y + \frac{e\mathcal{A}_y}{v_F}\right)\sigma_y\right]\boldsymbol{\psi} = E\boldsymbol{\psi}, \qquad (7)$$

where $\boldsymbol{\sigma}$ are Pauli matrices and $\boldsymbol{\psi} = (u_E^{(1)}(\boldsymbol{r}), v_E^{(1)}(\boldsymbol{r}))^T$ is a spinor associated with the BdG factors. For $\mathcal{A}_y$ linearly increasing along x the eigenstates are discrete Landau levels of energy $E_n = \pm \omega_c \sqrt{n}$, where $\omega_c = \sqrt{2ev_\Delta \partial_x \mathcal{A}_y(x)}$. The eigenstates at $1'$ are obtained via complex conjugation.

For *bona fide* magnetic fields it is well known [7] that Landau quantization generically leads to oscillations in thermodynamic and transport observables with applied field, most notably the de Haas–van Alphen and Shubnikov–de Haas effects. Similar effects have been predicted for strain-induced pseudomagnetic fields in Dirac [8] and Weyl materials [15]. These oscillations can be traced [7] to the dramatic enhancements in the total density of states (DOS) per unit volume whenever a LL crosses the Fermi energy. We argue that similar singularities arise in the present case and that the associated oscillations can be observed, in principle, in a suitable experimental setup. In the case of a clean superconductor under strain or doping gradient, a convenient way to probe the discrete nature of the LLs is to apply a small supercurrent to the sample, as indicated in Fig. 1(a). In the low-energy limit, the supercurrents induce an effective Doppler shift in quasiparticle energy [3] given by $E_{\boldsymbol{k}} \rightarrow E_{\boldsymbol{k}} + \boldsymbol{v}_s \cdot \boldsymbol{k}$, where $\boldsymbol{v}_s = \boldsymbol{q}_s/m$ defines the superfluid velocity [2]. This perturbation breaks time-reversal symmetry and, importantly, leads to opposite energy shifts around opposite momenta. We argue that this effect also occurs in the presence of strains or doping gradients. For fixed effective vector potentials, the DOS at the Fermi level will therefore exhibit sharp enhancements as a function of a weak, applied supercurrent. Similar effects are expected in the presence of fixed supercurrents and varying strain or doping gradients. In the following, we present numerical calculations which fully support our predictions.

III. NUMERICAL RESULTS

We model the lattice under strain via a slow variation of the hopping coefficients on the scale of the intersite spacing. For convenience, we consider pure shear strain as a function of x alone. The hopping coefficients are modulated as $t \rightarrow t(1 \pm l\delta_{sp})$ along the x and y directions, respectively, where l denotes the position along x and δ_{sp} is a small parameter. In the case of doping gradients we allow the chemical potential to vary as $\mu \rightarrow \mu(1 + l\delta_{dp})$ as a function of the x coordinate alone. Consequently, we impose periodic and open boundary conditions along the y and x axes, respectively. In the low-energy limit the modified coefficients lead to vector potentials [Eqs. (5) and (6)], corresponding to uniform pseudomagnetic fields only around the $(1, 1')$ pair of nodes (Appendix B).

We find the energy spectra of the modified lattice Hamiltonians numerically. All results are reported in units where $ta = 1$. The largest change in either hopping or chemical potential over the entire extent of the lattice is on the order of 10%. In Fig. 2(a) we show the low-energy spectrum as a function of k_y for the unperturbed d_{xy} superconductor around node 1. Note that the presence of the flat zero-energy dispersion is associated with topologically protected Majorana edge states [27] and is unrelated to the effect under discussion. In the presence of strain, the low-energy spectrum around the $(1, 1')$ pair of nodes is reorganized into discrete, flat bands, as illustrated in Fig. 2(b). The interlevel energy differences are those predicted by the Dirac-Landau spectrum. Similar effects are observed upon the inclusion of a weakly varying chemical potential, as shown in Fig. 2(c). The associated total DOS per unit area in the low-energy sectors, Figs. 2(d)–2(f), reflects the emergence of LLs.

In the presence of both strain and weak applied supercurrents the spectrum around the opposite $(1, 1')$ points is shifted to higher and lower energies, respectively, as shown in Figs. 3(a) and 3(b). An analogous behavior is obtained in the case of a doping gradient, as shown in Figs. 3(d) and 3(e). The total DOS per unit area in the presence of an applied supercurrent reflects the shifts in energies of the LLs. Most notably, it exhibits sharp enhancements whenever pairs of LLs around opposite nodes cross the Fermi energy. This is shown in Figs. 3(c) and 3(f) for a range of supercurrents for strain and doping gradient cases, respectively. Note that the applied supercurrent also lifts the degeneracy of the LLs and leads to a broadening of the sharp peaks in the DOS.

IV. SUMMARY AND OUTLOOK

We proposed that weak, slowly varying strains and doping gradients generically give rise to pseudomagnetic fields in the low-energy limit of two-dimensional nodal superconductors. For simplicity, our discussion was focused on a prototypical 2D d_{xy} SC. This is not essential, and similar effects are expected to occur in other types of SC which exhibit Dirac-like spectra around points in the Brillouin zone. Examples include $d_{x^2-y^2}$ cuprates and odd-parity p-wave cases. In view of similar proposals for pseudomagnetic fields in Weyl semimetals [10–15,28], such effects are also likely to occur in more complicated three-dimensional systems.
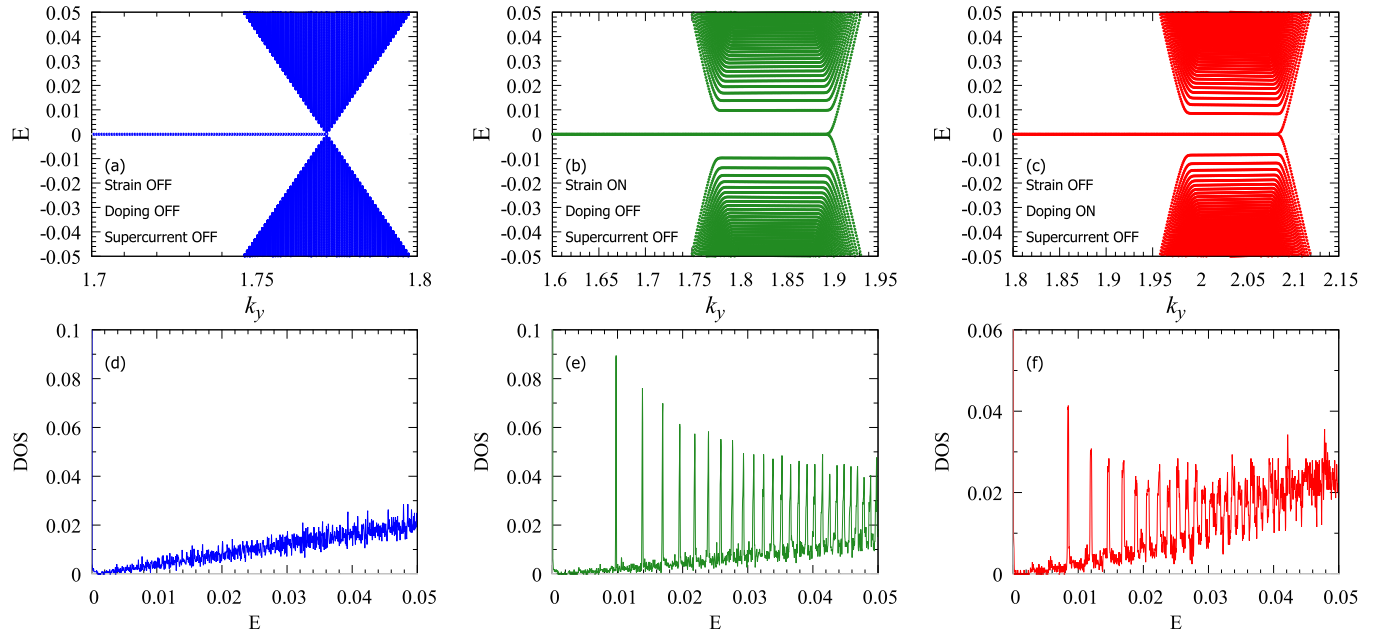
FIG. 2. Results of the numerical calculations for the 2D d_{xy} SC with and without the presence of strain and doping gradients. Computations were performed on a lattice with $L_x = 2000$ sites and $L_y = 8000$ crystal momentum points. We use $\Delta = 0.1$ and $\mu = -1.6$ and $\mu = -1.0$ for the strain and doping cases, respectively. (a) Low-energy spectrum around node 1 in the absence of both strain and doping gradients. (b) Same as in (a) with a finite pure-shear strain with $\delta_{sp} = 5 \times 10^{-5}$ which varies along the x direction. (c) Same as in (b) with a doping gradient $\delta_{dp} = 1 \times 10^{-4}$ instead of strain. (d)–(f) The total DOS per unit area for the cases in (a)–(c), respectively.

The most likely candidates for the experimental observation of such effects are the high-T_c cuprates. Specifically, in YBa$_2$Cu$_3$O$_x$ thin films and La$_{2-x}$Sr$_x$CuO$_4$−La$_2$CuO$_4$ bilayer samples, controlled doping gradients have recently been achieved [20,21]. According to our theory, such samples should already exhibit Landau level quantization which is, in

principle, observable as a series of sharp peaks in DOS through standard quasiparticle spectroscopies such as angle-resolved photoemission spectroscopy (ARPES) and scanning tunneling spectroscopy (STS). In the above samples a ∼10% doping variation is imposed over a millimeter scale, which allows us to estimate (Appendix C) the effective pseudomagnetic field
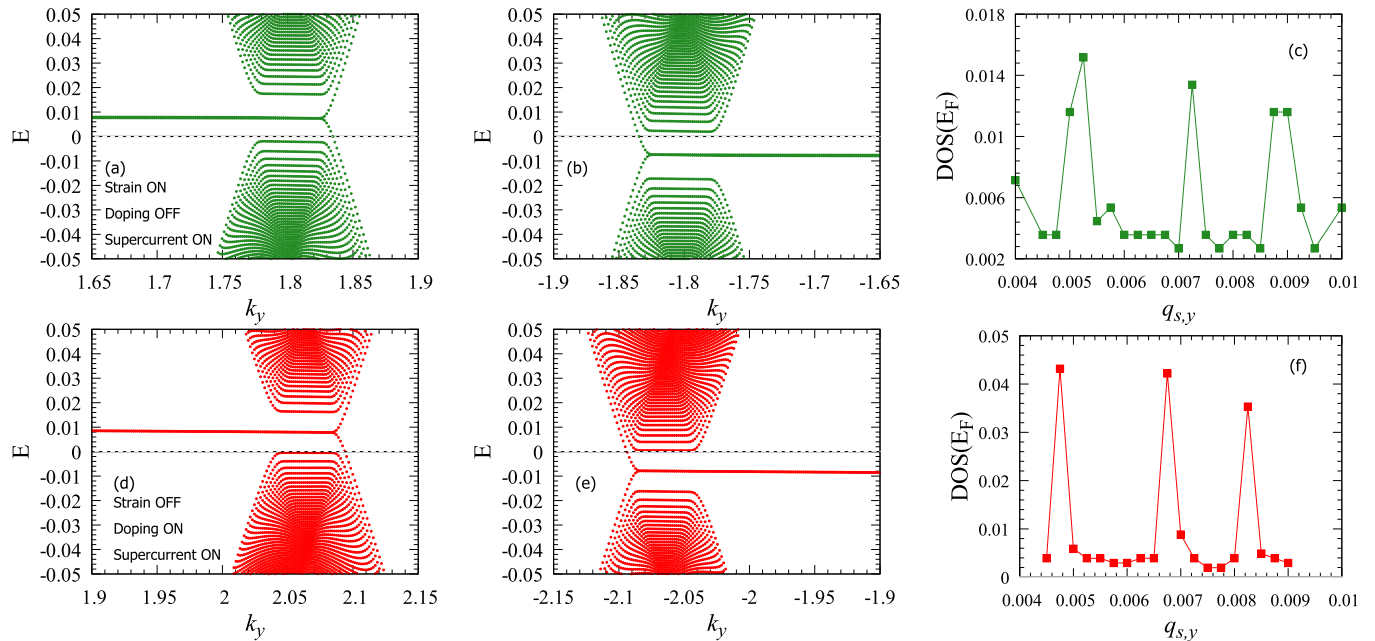
FIG. 3. Results of the numerical calculations for the 2D d_{xy} SC in the presence of strain and doping gradient and of an applied supercurrent. (a) The low-energy spectrum around node 1 in the presence of strain and of an applied supercurrent in the y direction. (b) Same as (a) for the opposite node, 1′. Note that the LLs have an opposite shift in energy with respect to node 1. (c) The DOS at the Fermi level E_F as a function of the applied supercurrent parameterized by the effective momentum $q_{s,y}$ [2]. The sharp spikes occur whenever a pair of LLs crosses the Fermi energy. (d)–(f) Same as (a)–(c) in the presence of a doping gradient alone.

as $\mathcal{B} \simeq 0.32$ mT and the Landau level spacing $\hbar\omega_c \simeq 82$ μeV. While this is probably too small to resolve by STS or ARPES, we see no fundamental reason why similar doping variations could not be imposed on a micrometer scale which would produce an effective field of the order of 1 T and clearly observable Landau levels. Under the applied supercurrent such samples would, in addition, show quantum oscillations in transport properties, such as the longitudinal thermal conductivity κ_{xx}. Large local strain gradients have recently been observed in nanocomposite $YBa_2Cu_3O_{7-\delta}$ films [19], which may afford an opportunity to study the effects discussed in this paper on a nanoscale, similar to the seminal work on "nanobubbles" in graphene [9].

The emergence of Landau levels in superconductors under strain and doping gradients naturally raises the question of quantized responses, by analogy with the integer quantum Hall effect. At this point, we can speculate that under appropriate conditions, these systems might exhibit exactly quantized thermal Hall conductance κ_{xy}. When the zero of the energy is tuned to lie between the bulk Landau levels by supercurrent as in Fig. 3, the electronic contribution to κ_{xx} vanishes. In this case, each bulk band is expected to carry a nonzero Chern number and produce a protected chiral edge mode, already visible in Fig. 3 as a dispersing feature terminating the flat Landau levels. More detailed considerations regarding thermal transport and other aspects related to possible nontrivial topology are relegated to future work.

Note added. Recently, we became aware of similar results reported in Ref. [29].

APPENDIX A: LOW-ENERGY CONTINUUM LIMIT IN THE PRESENCE OF ARBITRARY DEFORMATIONS AND DOPING GRADIENTS

The Hamiltonian on the two-dimensional square lattice is given by

$$\hat{H} = \hat{H}_{TB} + \hat{H}_\Delta, \tag{A1}$$

where $\hat{H}_{TB}$ is a nearest-neighbor (NN) tight-binding part and $\hat{H}_\Delta$ is a pairing part corresponding to a d_{xy} irreducible representation of the D_{4h} point group.

1. Tight-binding part in the presence of an arbitrary deformation

In the absence of strain, the TB part is given by

$$\hat{H}_{TB} = \sum_i \left[\sum_{j \in \langle ij \rangle} \sum_\sigma t(\boldsymbol{\delta}_j) c_\sigma^\dagger(\boldsymbol{R}_i) c_\sigma(\boldsymbol{R}_i + \boldsymbol{\delta}_j) + \text{H.c.} \right] \\ - \sum_i \mu c_\sigma^\dagger(\boldsymbol{R}_i) c_\sigma(\boldsymbol{R}_i), \tag{A2}$$

where σ is a spin index which is ignored for the rest of this section. $\boldsymbol{R}_i$ are the Bravais lattice vectors, while $\boldsymbol{\delta}_j \in \{(a,0),(0,a)\}$ are the vectors which connect NNs, a is the NN distance, and μ is the chemical potential. The latter is chosen

such that the system is below half filing. $\hat{H}_{TB}$ is diagonalized by applying a Fourier transform,

$$c(\boldsymbol{R}_i) = \frac{1}{\sqrt{N}} \sum_{k \in BZ} e^{ik \cdot \boldsymbol{R}_i} c_{\boldsymbol{k}}, \tag{A3}$$

where N is the number of unit cells.

In the presence of a lattice deformation, the lattice TB Hamiltonian undergoes the transformation

$$\boldsymbol{R}_i \rightarrow \boldsymbol{R}_i' = \boldsymbol{R}_i + \boldsymbol{u}(\boldsymbol{R}_i), \tag{A4}$$

where $\boldsymbol{u}(\boldsymbol{R}_i)$ is a position-dependent displacement. In general, the hopping coefficients are modified accordingly:

$$t(\boldsymbol{\delta}_j) \rightarrow t'(\boldsymbol{\delta}_j) = t[\boldsymbol{R}_i + \boldsymbol{\delta}_j + \boldsymbol{u}(\boldsymbol{R}_i + \boldsymbol{\delta}_j) - \boldsymbol{R}_i - \boldsymbol{u}(\boldsymbol{R}_i)]$$
$$= t[\boldsymbol{\delta}_j + \boldsymbol{u}(\boldsymbol{R}_i + \boldsymbol{\delta}_j) - \boldsymbol{u}(\boldsymbol{R}_i)]. \tag{A5}$$

We assume that the hopping coefficients can be approximated by continuous functions of the displacement. The transformed Hamiltonian is

$$\hat{H}_{TB} \rightarrow \hat{H}_{TB}' = \sum_i \left\{ \sum_{j \in \langle ij \rangle} t[\boldsymbol{\delta}_j + \boldsymbol{u}(\boldsymbol{R}_i + \boldsymbol{\delta}_j) - \boldsymbol{u}(\boldsymbol{R}_i)]c^\dagger \right. $$
$$ \times [\boldsymbol{R}_i + \boldsymbol{u}(\boldsymbol{R}_i)]c[\boldsymbol{R}_i + \boldsymbol{u}(\boldsymbol{R}_i + \boldsymbol{\delta}_j) $$
$$ \left. + \boldsymbol{\delta}_j] + \text{H.c.} \right\} - \sum_i \mu c^\dagger[\boldsymbol{R}_i + \boldsymbol{u}(\boldsymbol{R}_i)] $$
$$ \times c[\boldsymbol{R}_i + \boldsymbol{u}(\boldsymbol{R}_i)]. \tag{A6}$$

We consider the low-energy continuum limit of $\hat{H}_{TB}'$. Consequently, we approximate the lattice operators as products of parts which vary rapidly and slowly on the scale of the lattice as

$$c(\boldsymbol{R}_i) \approx \sum_\alpha e^{i\boldsymbol{K}_\alpha \cdot \boldsymbol{R}_i} \Psi^{(\alpha)}(\boldsymbol{R}_i), \tag{A7}$$

where $\Psi^{(\alpha)}(\boldsymbol{R}_i)$ is a slowly varying Fermi field and $\alpha \in \{1,1',2,2'\}$ represents the positions of the four nodes at Fermi wave vectors $\boldsymbol{K}_\alpha \in \{(0, \pm K_F),(\pm, K_F, 0)\}$. We assume that the lattice displacements can be approximated by a continuous displacement field:

$$\boldsymbol{R}_i + u(\boldsymbol{R}_i) \rightarrow \boldsymbol{r} + \boldsymbol{u}(\boldsymbol{r}). \tag{A8}$$

On the scale of the lattice, variations in the displacements can be approximated by

$$\boldsymbol{u}(\boldsymbol{r} + \boldsymbol{\delta}_j) \approx \boldsymbol{u}(\boldsymbol{r}) + (\boldsymbol{\delta}_j \cdot \nabla)\boldsymbol{u}(\boldsymbol{r}). \tag{A9}$$

In the following, we expand the continuum limit of the Hamiltonian in terms of leading gradient terms.

It should be noted that such an expansion is valid provided that the gradient term in Eq. (A9) remains small throughout. As discussed in the following, in order to obtain finite pseudomagnetic fields we consider deformation gradients which vary monotonically. This implicitly introduces a spatial scale at which these gradients are no longer small. Therefore, the effective continuum approximation only holds provided that the deformation at any point of a sample of finite extent remains small.

Applying the above to $\hat{H}'_{TB}$, we obtain

$$\hat{H}'_{TB} = \int d^2r \sum_\alpha \Psi^{\dagger,(\alpha)}(\boldsymbol{r}+\boldsymbol{u})\bigg\{\sum_j 2t[\boldsymbol{\delta}_j + (\boldsymbol{\delta}_j \cdot \boldsymbol{\nabla})\boldsymbol{u}][\cos\{\boldsymbol{K}_\alpha \cdot [\boldsymbol{\delta}_j + (\boldsymbol{\delta}_j \cdot \boldsymbol{\nabla})\boldsymbol{u}]\}$$

$$+ i\sin\{\boldsymbol{K}_\alpha \cdot [\boldsymbol{\delta}_j + (\boldsymbol{\delta}_j \cdot \boldsymbol{\nabla})\boldsymbol{u}]\}(\boldsymbol{\delta}_j \cdot \boldsymbol{\nabla})]\bigg\}\Psi^{(\alpha)}(\boldsymbol{r}+\boldsymbol{u}) - \mu\sum_\alpha \int d^2r \Psi^{\dagger,(\alpha)}(\boldsymbol{r}+\boldsymbol{u})\Psi^{(\alpha)}(\boldsymbol{r}+\boldsymbol{u}), \tag{A10}$$

where we neglected internode terms. The explicit dependence of the fields on $\boldsymbol{u}$ can be formally eliminated via a coordinate transformation,

$$\boldsymbol{r}' = \boldsymbol{r} + \boldsymbol{u}(\boldsymbol{r}), \tag{A11}$$

with a Jacobian $1 + u_{ii}$, where $u_{ij} = \partial_j u_i$ and implicit summation is assumed. We also approximate $\boldsymbol{\delta}_j \cdot \boldsymbol{\nabla} u(\boldsymbol{r}) \approx \boldsymbol{\delta}_j \cdot \boldsymbol{\nabla} u(\boldsymbol{r}')$ and expand the following terms:

$$t[\boldsymbol{\delta}_j + (\boldsymbol{\delta}_j \cdot \boldsymbol{\nabla})\boldsymbol{u}] \approx t(\boldsymbol{\delta}_j) + (\boldsymbol{\delta}_j \cdot \boldsymbol{\nabla})\boldsymbol{u} \cdot \boldsymbol{\nabla} t(\boldsymbol{\delta}_j), \tag{A12}$$

$$\cos\{\boldsymbol{K}_\alpha \cdot [\boldsymbol{\delta}_j + (\boldsymbol{\delta}_j \cdot \boldsymbol{\nabla})\boldsymbol{u}]\} \approx \cos(\boldsymbol{K}_\alpha \cdot \boldsymbol{\delta}_j) - \boldsymbol{K}_\alpha \cdot (\boldsymbol{\delta}_j \cdot \boldsymbol{\nabla})\boldsymbol{u}\sin(\boldsymbol{K}_\alpha \cdot \boldsymbol{\delta}_j), \tag{A13}$$

$$\sin\{\boldsymbol{K}_\alpha \cdot [\boldsymbol{\delta}_j + (\boldsymbol{\delta}_j \cdot \boldsymbol{\nabla})\boldsymbol{u}]\} \approx \sin(\boldsymbol{K}_\alpha \cdot \boldsymbol{\delta}_j) + \boldsymbol{K}_\alpha \cdot (\boldsymbol{\delta}_j \cdot \boldsymbol{\nabla})\boldsymbol{u}\cos(\boldsymbol{K}_\alpha \cdot \boldsymbol{\delta}_j). \tag{A14}$$

To zeroth order in the gradient expansion we obtain

$$H_{TB}^{(0)} = \int d^2r \sum_\alpha \sum_j 2t(\boldsymbol{\delta}_j)\Psi^{\dagger,(\alpha)}(\boldsymbol{r})\{\cos(\boldsymbol{K}_\alpha \cdot \boldsymbol{\delta}_j) + i\sin(\boldsymbol{K}_\alpha \cdot \boldsymbol{\delta}_j)(\boldsymbol{\delta}_j \cdot \boldsymbol{\nabla})\}\Psi^{(\alpha)}(\boldsymbol{r})\mu\sum_\alpha \int d^2r \Psi^{\dagger,(\alpha)}(\boldsymbol{r})\Psi^{(\alpha)}(\boldsymbol{r}). \tag{A15}$$

The first and last terms cancel since $\boldsymbol{K}_\alpha$ is on the Fermi surface. The second term gives the leading linear dispersion and also defines the Fermi velocity $v_F = 2ta\sin(K_F a)$.

To first order, we obtain

$$H_{TB}^{(1)} = \sum_\alpha \sum_j \bigg\{\int d^2r(u_{xx}+u_{yy})2t(\boldsymbol{\delta}_j)\cos(\boldsymbol{K}_\alpha \cdot \boldsymbol{\delta}_j) + \int d^2r2(\boldsymbol{\delta}_j \cdot \boldsymbol{\nabla})\boldsymbol{u} \cdot \boldsymbol{\nabla} t\cos(\boldsymbol{K}_\alpha \cdot \boldsymbol{\delta}_j)$$

$$+ \int d^2r2t(\boldsymbol{\delta}_j)[-\boldsymbol{K}_\alpha \cdot (\boldsymbol{\delta}_j \cdot \boldsymbol{\nabla})\boldsymbol{u}\sin(\boldsymbol{K}_\alpha \cdot \boldsymbol{\delta}_j)]\bigg\}\Psi^{\dagger,(\alpha)}(\boldsymbol{r})\Psi^{(\alpha)}(\boldsymbol{r}) - \mu\sum_\alpha \int d^2r(u_{xx}+u_{yy})\Psi^{\dagger,(\alpha)}(\boldsymbol{r})\Psi^{(\alpha)}(\boldsymbol{r}). \tag{A16}$$

The first two terms cancel independently of the details of the deformation. They represent local dilation/contraction with all other parameters fixed. The expression can be simplified further by carrying out the summations over NNs. The result is summarized by

$$H_{TB}^{(1)} = \sum_\alpha \int d^2r e\mathcal{A}^\alpha(\boldsymbol{r})\Psi^{\dagger,(\alpha)}(\boldsymbol{r})\Psi^{(\alpha)}(\boldsymbol{r}), \tag{A17}$$

where the electron charge e was introduced for dimensional consistency. The effective *vector* potentials around either the 1 node or the 1' node are defined as

$$\mathcal{A}^{(1,1')} = \begin{pmatrix} 0 \\ \left(\frac{2a}{e}\right)\{t'_\parallel u_{xx} + t'_\perp u_{yx} + t'_\perp \cos(K_F a)u_{xy} + [t'_\parallel \cos(K_F a) - tK_F \sin(K_F a)]u_{yy}\} \end{pmatrix}. \tag{A18}$$

The $\mathcal{A}_x$ component is formally set to zero since there is no linear-derivative term along the x direction to leading order for the TB part. We also defined the coefficients $\partial_x t_x = \partial_y t_y = t'_\parallel, \partial_x t_y = \partial_y t_x = t'_\perp$, which are restricted by the symmetry of the square lattice, while, in general, $t'_\perp \neq t'_\parallel$. The analogous nontrivial vector potentials $\mathcal{A}_x$ around the other pair of Fermi momenta can be obtained by replacing $x \leftrightarrow y$.

2. Pairing part in the presence of an arbitrary deformation

In the absence of any deformation, the paring part of the Hamiltonian for a 2D d_{xy} SC is given by

$$\hat{H}_\Delta = \sum_i \sum_{j\in\langle\langle ij \rangle\rangle} \sum_\sigma \sum_{\sigma'} \Delta_{\sigma\sigma'}(\boldsymbol{\delta}_j)[c_\sigma(\boldsymbol{R}_i)c_{\sigma'}(\boldsymbol{R}_i + \boldsymbol{\delta}_j) + c_\sigma(\boldsymbol{R}_i)c_{\sigma'}(\boldsymbol{R}_i - \boldsymbol{\delta}_j)] + \text{H.c.}, \tag{A19}$$

where the pairing occurs for next-nearest-neighbor (NNN) sites, $\Delta_{\sigma\sigma'}(\boldsymbol{\delta}_j) = \Delta(\boldsymbol{\delta}_j)i\sigma_y$, corresponding to even-parity, spin-singlet pairing. In addition, $\Delta(\boldsymbol{\delta}_{1/2}) = \pm\Delta$, with $\boldsymbol{\delta}_{1/2} = (\pm a, a)$ determining the vectors which connect NNNs.

We allow for the deformation given by Eq. (A8) and assume that its effect on the pairing potential can be generically captured to lowest order in the strains. The derivation of the low-energy continuum limit is analogous to that of the TB part. We list the final results for the $(1,1')$ pair of nodes:

$$H_\Delta^{(0)} = \int d^2r \sum_{(\alpha,\beta)} 4a\Delta_{\sigma\sigma'} \sin\left(K_{Fy,\alpha}a\right)\Psi_\sigma^\alpha(\boldsymbol{r})(-i\partial_x)\Psi_{\sigma'}^\beta(\boldsymbol{r}) + \text{H.c.}, \tag{A20}$$

$$H_\Delta^{(1)} = \int d^2r \sum_{(\alpha,\beta)} \sum_{\sigma,\sigma'} (-i\sigma_y)_{\sigma,\sigma'} 4a[(u_{xx}\partial_x\Delta + u_{yx}\partial_y\Delta)\cos(K_Fa) - \Delta K_F u_{yx}\sin(K_Fa)]\Psi_\sigma^\alpha(\boldsymbol{r})\Psi_{\sigma'}^\beta(\boldsymbol{r}), \tag{A21}$$

where $\alpha \neq \beta$. The zeroth-order term defines a velocity $v_\Delta = 4a\Delta\sin(K_Fa)$. For the $(2,2')$ pair, we replace $x \leftrightarrow y$. We can also set $\partial_x\Delta = \partial_y\Delta = \Delta'$.

3. Effective gauge potentials in the presence of strain

The first-order corrections to the pairing part can be eliminated via the gauge transformation

$$\Psi_{\sigma'}^\beta \rightarrow \Psi_{\sigma'}^\beta e^{-i\,\text{sgn}(K_{Fy,\alpha})\frac{\phi(\boldsymbol{r})}{v_\Delta}}, \tag{A22}$$

where

$$\phi = 4a\Delta'(u_x + u_y)\cos(K_{F,\alpha}a) - \Delta K_F u_y \sin(K_Fa). \tag{A23}$$

The transformation modifies $\mathcal{A}_y$ in Eq. (A18) to

$$\mathcal{A}_y' = \mathcal{A}_y - \frac{v_F}{v_\Delta e}\partial_y\phi. \tag{A24}$$

The terms proportional to $\sin(K_Fa)$ cancel. The expression for the most general gauge-strain-induced vector potentials for the $(1,1')$ fields reduces to

$$\mathcal{A}_y = \left(\frac{2a}{e}\right)\left\{t_\parallel' u_{xx} + \left[t_\parallel' - \left(\frac{t}{\Delta}\right)\Delta'\right]\cos(K_Fa)u_{yy}\right.$$
$$\left. + t_\perp' u_{yx} + \left[t_\perp' - \left(\frac{t}{\Delta}\right)\Delta'\right]\cos(K_Fa)u_{xy}\right\}. \tag{A25}$$

The corresponding $\mathcal{A}_x$ for the $(2,2')$ pair is obtained by replacing $x \leftrightarrow y$. Note that $t_\parallel'$ corresponds to a change in bond length, and $t_\perp'$ corresponds to a change in bond angle, while Δ' includes both. In the most general case, the coefficients depend on the details of the model, in particular on the symmetry of the orbitals.

Note that arbitrary strain $u_{ij}(x,y)$ always enters the low-energy theory through a minimally coupled $\mathcal{A}_y$ component of the vector potential as in Eq. (A25). This surprising result can be understood when one considers the gauge transformation of Eq. (A22), which introduces the nontrivial phases $\text{sgn}(K_{Fy,\alpha})\frac{\phi(\boldsymbol{r})}{v_\Delta}$. These incorporate the effects of strain on the pairing amplitude in the low-energy limit and account for the "missing" $\mathcal{A}_x$ component. To see this more clearly, we can consider the case of linear-in-position strains. The phases defined by Eqs. (A22) and (A23) provide an additional modulation of the low-energy wave functions and thus represent effective shifts in the position of nodes 1 and 1' in the Brillouin zone.

We focus on cases where the dominant contribution comes from the change in bond length, i.e., $t_\parallel' \neq 0, t_\perp' \approx 0$. Such an approximation can be justified, in principle, using a Slater-Koster scheme [30] and is consistent with the similar case of graphene [31]. Additionally, we assume that the leading change in the pairing potential under strain Δ is also negligible. Under

these assumptions and writing

$$at_\parallel' = t\frac{d\ln t}{d\ln a} = t\beta, \tag{A26}$$

we obtain the form of the vector potentials discussed in the main text.

4. Effective gauge potentials from doping gradients

We consider the effect of a doping gradient $\mu \rightarrow \mu(\boldsymbol{R}_i)$ on the Hamiltonian of Eq. (A1). The low-energy continuum limit in this case is

$$H = H_{TB}^{(0)} + H_\Delta^{(0)} + H_{dg}, \tag{A27}$$

where the first two terms correspond to the unperturbed Hamiltonians for the TB and pairing parts, given by Eqs. (A15) and (A20), respectively. The last term is the contribution of a spatially varying chemical potential,

$$H_{dg} = -e\sum_\alpha \int d^2r\left(\frac{\tilde{\mu}(\boldsymbol{r})}{e}\right)\Psi^{\dagger,(\alpha)}(\boldsymbol{r})\Psi^{(\alpha)}(\boldsymbol{r}), \tag{A28}$$

where

$$\tilde{\mu}(\boldsymbol{r}) = \mu g(\boldsymbol{r}). \tag{A29}$$

The corresponding vector potential around the $(1,1')$ pair of nodes is

$$\mathcal{A}^{(1,1')} = \begin{pmatrix} 0 \\ \left(\frac{\mu}{e}\right)g(\boldsymbol{r}) \end{pmatrix}, \tag{A30}$$

with an analogous $\mathcal{A}_x$ around $(2,2')$. These vector potentials must remain small throughout the finite area of the sample and are subject to the constraints imposed in the case of strain.

5. Low-energy Nambu form of the Hamiltonian in the presence of nontrivial vector potentials

In either strain or doping cases, we can write the Hamiltonian in the low-energy sector as

$$H = \int d^2r \begin{pmatrix} \Psi_\uparrow^{\dagger,(1)} \\ \Psi_\downarrow^{\dagger,(1')} \\ \Psi_\uparrow^{(1)} \\ \Psi_\downarrow^{(1')} \end{pmatrix}^T \begin{pmatrix} v_F\left(i\partial_y + e\frac{\mathcal{A}_y}{v_F}\right) & 0 & 0 & v_\Delta(-i\partial_x) \\ 0 & v_F\left(-i\partial_y + e\frac{\mathcal{A}_y}{v_F}\right) & v_\Delta(-i\partial_x) & 0 \\ 0 & v_\Delta(-i\partial_x) & v_F\left(i\partial_y - e\frac{\mathcal{A}_y}{v_F}\right) & 0 \\ v_\Delta(-i\partial_x) & 0 & 0 & v_F\left(-i\partial_y - e\frac{\mathcal{A}_y}{v_F}\right) \end{pmatrix} \begin{pmatrix} \Psi_\uparrow^{(1)} \\ \Psi_\downarrow^{(1')} \\ \Psi_\uparrow^{\dagger,(1)} \\ \Psi_\downarrow^{\dagger,(1')} \end{pmatrix},$$

(A31)

which is identical to Eq. (4) of the main text. With vanishing vector potentials, one can easily check that this is the low-energy continuum limit of the Hamiltonian of Eq. (1) of the main text:

$$H = \sum_k \begin{pmatrix} c_{k\uparrow}^\dagger \\ c_{-k\downarrow} \end{pmatrix}^T \begin{pmatrix} h_k & \Delta_k \\ \Delta_k & -h_k \end{pmatrix} \begin{pmatrix} c_{k\uparrow} \\ c_{-k\downarrow}^\dagger \end{pmatrix} + \begin{pmatrix} c_{k\downarrow}^\dagger \\ c_{-k\uparrow} \end{pmatrix}^T \begin{pmatrix} h_k & -\Delta_k \\ -\Delta_k & -h_k \end{pmatrix} \begin{pmatrix} c_{k\downarrow} \\ c_{-k\uparrow}^\dagger \end{pmatrix}.$$

(A32)

The BdG equations can be obtained in the standard fashion by considering the block Hamiltonian

$$H' = \int d^2r \begin{pmatrix} \Psi_\downarrow^{\dagger,(1')} \\ \Psi_\uparrow^{(1)} \end{pmatrix}^T \begin{pmatrix} v_F\left(-i\partial_y + e\frac{\mathcal{A}_y}{v_F}\right) & v_\Delta(-i\partial_x) \\ v_\Delta(i\partial_x) & v_F\left(i\partial_y - e\frac{\mathcal{A}_y}{v_F}\right) \end{pmatrix} \begin{pmatrix} \Psi_\downarrow^{(1')} \\ \Psi_\uparrow^{\dagger,(1)} \end{pmatrix},$$

(A33)

together with the fact that $\Psi_\downarrow^{(1')}, \Psi_\uparrow^{(1)}$ are related through time reversal. The remaining sector can also be obtained via the same operation.

APPENDIX B: NUMERICAL CALCULATIONS

For the purpose of numerical computation, we introduce position-dependent tight-binding coefficients or chemical potentials at the level of the Hamiltonian in Eq. (A1). Moreover, these vary slowly on the scale of the lattice. Depending on the spatial dependence of these parameters, we recover the different cases discussed in the main text.

In practice, we allow a nontrivial spatial variation along the x direction but keep periodic boundary conditions along y.

1. Deformation-induced vector potentials

In this case, we choose

$$t(\boldsymbol{\delta}_j) \to t(\boldsymbol{\delta}_j)[1 + f(\boldsymbol{R}_i, \boldsymbol{\delta}_j)]. \tag{B1}$$

In the low-energy continuum approximation, the corrections to the hopping coefficients are analogous to the second term in Eq. (A16), which is the contribution of the transformed TB coefficients:

$$H_{TB}^{(1)} = \sum_\alpha \sum_j \int d^2r\, 2tf(\boldsymbol{r}, \boldsymbol{\delta}_j) \cos(\boldsymbol{K}_\alpha \cdot \boldsymbol{\delta}_j)$$
$$\times \Psi^{\dagger,(\alpha)}(\boldsymbol{r})\Psi^{(\alpha)}(\boldsymbol{r}). \tag{B2}$$

We consider the three limiting cases discussed in the main text:

(i) *Uniaxial strain along the x axis.* This corresponds to $f(x, \boldsymbol{\delta}_x) \neq 0$, with the component in the y direction equal to zero. The vector potential is $\mathcal{A}_y = tf(x, \boldsymbol{\delta}_x)$ for the $(1, 1')$ pair of nodes, and $\mathcal{A}_y = 0$ for the other pair. On the lattice this amounts to $f(x_l, \boldsymbol{\delta}_x) = l\delta_{sp}$, where $\delta_{sp} \ll 1$.

(ii) *Hydrostatic compression/dilatation.* In this case, the finite vector potentials about each pair of nodes are equal. We take $f(x, \boldsymbol{\delta}_x) = f(x, \boldsymbol{\delta}_y) = f(x)$. The dependence on x alone is purely for computational convenience. The resulting vector potentials are $\mathcal{A}_{x/y} = 2tf(x)[1 + \cos(K_Fa)]$. On the lattice, we have $f(x_l, \boldsymbol{\delta}_x) = l\delta_{sp}$.

(iii) *Pure shear deformation.* We choose $f(x, \boldsymbol{\delta}_x) = -f(x, \boldsymbol{\delta}_y)$. The vector potentials are $\mathcal{A}_{y/x} = \pm 2tf(x)[1 - \cos(K_Fa)]$. On the lattice, we have $f(x_l, \boldsymbol{\delta}_x) = l\delta_{sp}$, with a corresponding negative sign for hopping along the y direction.

2. Doping-gradient-induced vector potentials

This case is qualitatively similar to that of a deformation since $\tilde{\mu}(\boldsymbol{r}) = \mu g(\boldsymbol{r})$. In practice, we take $g(\boldsymbol{r}) = g(x)$. On the lattice, this amounts to $g(x_l) = l\delta_{dp}$, with $\delta_{dp} \ll 1$.

APPENDIX C: ESTIMATE OF DOPING-GRADIENT-INDUCED LANDAU LEVEL SPACING AND PSEUDOMAGNETIC FIELDS

We estimate that the candidate cuprate films are generically characterized by the parameters (1) $\Delta \approx 30$ meV [32], (244) $a \approx 3.9$ Å, (3) $K_Fa \approx \pi/2$, (4) $t \approx 0.38$ eV [33], and (5) $\mu \approx 1.52$ eV as determined from $\mu \approx 2t[1 + \cos(K_Fa)] \approx 4t$. In addition, we estimate $\partial_x g(x) \approx 0.047$ mm^{-1} from the relative variation in the hole concentration $\partial_x g(x) \approx (\Delta p)/(p_0 \Delta x)$ over the sample length in Ref. [20]. The rate in Ref. [21] is roughly half of this. Upon including factors of $\hbar$ for dimensional consistency we obtain

$$E_{c,\text{Doping}} = \sqrt{8\Delta\mu a[\sin(K_Fa)]\partial_x g(x)}, \tag{C1}$$

$$\mathcal{B}_{\text{Doping}} = \frac{\Phi_0}{2\pi} \frac{\mu \partial_x g}{2ta \sin(K_Fa)} \tag{C2}$$

for the inter-LL spacing and pseudomagnetic field, respectively. Note that $\Phi_0 = hc/e = 4.12 \times 10^5$ T Å^2 is the quantum of flux.

[1] J. Bardeen, L. N. Cooper, and J. R. Schrieffer, Phys. Rev. **106**, 162 (1957).

[2] P. G. de Gennes, *Superconductivity of Metals and Alloys* (Westview, Boulder, 1999).

[3] M. Tinkham, *Introduction to Superconductivity* (McGraw-Hill, New York, 1996).

[4] W. Meissner and R. Ochsenfeld, Naturwissenschaften **21**, 787 (1933).

[5] A. A. Abrikosov, Sov. Phys. JETP **5**, 1174 (1957).

[6] M. Franz and Z. Tesanovic, Phys. Rev. Lett. **84**, 554 (2000).

[7] D. Shoenberg, *Magnetic Oscillations in Metals* (Cambridge University Press, Cambridge, 1984).

[8] F. Guinea, M. I. Katsnelson, and A. K. Geim, Nat. Phys. **6**, 30 (2009).

[9] N. Levy, S. A. Burke, K. L. Meaker, M. Panlasigui, A. Zettl, F. Guinea, A. H. C. Neto, and M. F. Crommie, Science **329**, 544 (2010).

[10] H. Shapourian, T. L. Hughes, and S. Ryu, Phys. Rev. B **92**, 165131 (2015).

[11] A. Cortijo, Y. Ferreiros, K. Landsteiner, and M. A. H. Vozmediano, Phys. Rev. Lett. **115**, 177202 (2015).

[12] H. Sumiyoshi and S. Fujimoto, Phys. Rev. Lett. **116**, 166601 (2016).

[13] D. I. Pikulin, A. Chen, and M. Franz, Phys. Rev. X **6**, 041021 (2016).

[14] A. G. Grushin, J. W. F. Venderbos, A. Vishwanath, and R. Ilan, Phys. Rev. X **6**, 041046 (2016).

[15] T. Liu, D. I. Pikulin, and M. Franz, Phys. Rev. B **95**, 041201(R) (2017).

[16] B. Uchoa and Y. Barlas, Phys. Rev. Lett. **111**, 046604 (2013).

[17] I. Bozovic, G. Logvenov, I. Belca, B. Narimbetov, and I. Sveklo, Phys. Rev. Lett. **89**, 107001 (2002).

[18] A. Chen, J.-M. Hu, P. Lu, T. Yang, W. Zhang, L. Li, T. Ahmed, E. Enriquez, M. Weigand, Q. Su, H. Wang, J.-X. Zhu, J. L. MacManus-Driscoll, L.-Q. Chen, D. Yarotski, and Q. Jia, Sci. Adv. **2**, e1600245 (2016).

[19] R. Guzman, J. Gazquez, B. Mundet, M. Coll, X. Obradors, and T. Puig, Phys. Rev. Mater. **1**, 024801 (2017).

[20] B. J. Taylor, C. A. McElroy, I. K. Lum, A. M. L. de Escobar, M. C. de Andrade, T. J. Wong, E. Y. Cho, and M. B. Maple, Phys. Rev. B **91**, 144511 (2015).

[21] J. Wu, O. Pelleg, G. Logvenov, A. T. Bollinger, Y.-J. Sun, G. S. Boebinger, M. Vanević, Z. Radović, and I. Božović, Nat. Mater. **12**, 877 (2013).

[22] S. H. Simon and P. A. Lee, Phys. Rev. Lett. **78**, 1548 (1997).

[23] H. Suzuura and T. Ando, Phys. Rev. B **65**, 235412 (2002).

[24] M. A. H. Vozmediano, M. I. Katsnelson, and F. Guinea, Phys. Rep. **496**, 109 (2010).

[25] J. L. Manes, Phys. Rev. B **76**, 045430 (2007).

[26] J. L. Manes, F. de Juan, M. Sturla, and M. A. H. Vozmediano, Phys. Rev. B **88**, 155405 (2013).

[27] A. C. Potter and P. A. Lee, Phys. Rev. Lett. **112**, 117002 (2014).

[28] T. Liu, M. Franz, and S. Fujimoto, Phys. Rev. B **96**, 224518 (2017).

[29] G. Massarelli, G. Wachtel, J. Y. T. Wei, and A. Paramekanti, Phys. Rev. B **96**, 224516 (2017); L. D. Landau and E. M. Lifshitz, *Theory of Elasticity* (Pergamon, New York, 1970).

[30] J. C. Slater and G. F. Koster, Phys. Rev. **94**, 1498 (1954).

[31] A. H. Castro, F. Guinea, N. M. R. Peres, K. S. Novoselov, and A. K. Geim, Rev. Mod. Phys. **81**, 109 (2009).

[32] M. Hashimoto, I. M. Vishik, R.-H. He, T. P. Devereaux, and Z.-X. Shen, Nat. Phys. **10**, 483 (2014).

[33] M. M. Korshunov, V. A. Gavrichkov, S. G. Ovchinnikov, D. Manske, and I. Eremin, Phys. C **402**, 365 (2004).